

Supporting Information

Efficient solid and solution state emissive reusable solvatochromic fluorophore for colorimetric and fluorometric detection of CN⁻

Atanu Maji, Krishnendu Aich, Amitav Biswas, Saswati Gharami, Biswajit Bera and Tapan K. Mondal^{†,*}

[†]*Department of Chemistry, Jadavpur University, Kolkata- 700032, India. E-mail: tapank.mondal@jadavpuruniversity.in*

CONTENTS

- Fig. S1. ¹H-NMR spectrum of CPI
- Fig. S2. ¹³C-NMR spectra of CPI
- Fig. S3. ESI mass spectra of CPI
- Fig. S4. IR- spectra of CPI
- Fig. S5. Change in UV-Vis spectra of the probe (CPI) (20 μM) upon addition of 2 equivalent of various anions (40 μM)
- Fig. S6. Change in emission spectra of the probe (CPI) (20 μM) upon addition of 2 equivalent of various anions (40 μM)
- Fig. S7. Competitive experiments of CPI for CN⁻ in presence of common anions.
- Fig. S8. Stoichiometry plot of CPI for CN⁻
- Fig. S9. Linear response curve of CPI depending on CN⁻ ion concentration.
- Fig. S10. pH study of CPI for CN⁻
- Fig. S11. Lifetime decay profile of CPI and CPI-CN⁻
- Table S1. Determination of quantum yield, radiative and non-radiative rate constant of CPI and CPI-CN⁻
- Fig. S12: Mole ratio plot of CPI for CN⁻
- Fig. S 13: Photostability plot of CPI and CPI-CN⁻
- Fig. S 14: FTIR spectra of CPI and CPI-CN⁻
- Fig. S15. Optimized structure of CPI calculated by DFT/B3LYP/6-31+G(d) method
- Fig. S16. Optimized structure of CPI-CN⁻ calculated by DFT/B3LYP/6-31+G(d) method
- Table S2. Crystallographic data and refinement parameters of the sensor (CPI)
- Table S3. Selected X-ray and calculated bond distances and angles of the probe (CPI)
- Fig. S17. Contour plots of some selected molecular orbitals of CPI
- Fig. S18. Contour plots of some selected molecular orbitals of CPI⁻
- Table S4. Vertical electronic transitions calculated by TDDFT/B3LYP/CPCM method for CPI in DMSO.
- Table S5. Sensing performance of CPI towards CN⁻ compared to others previously reported receptors.

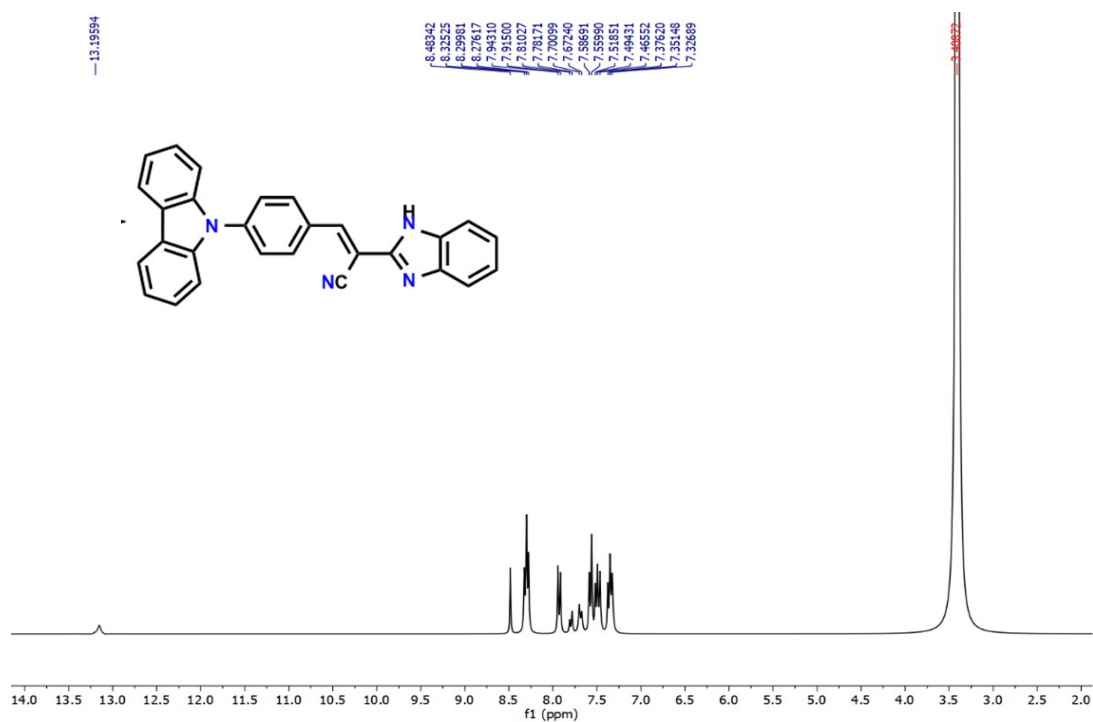


Figure S1: ^1H NMR (300 MHz) spectra of the probe CPI in DMSO-d_6

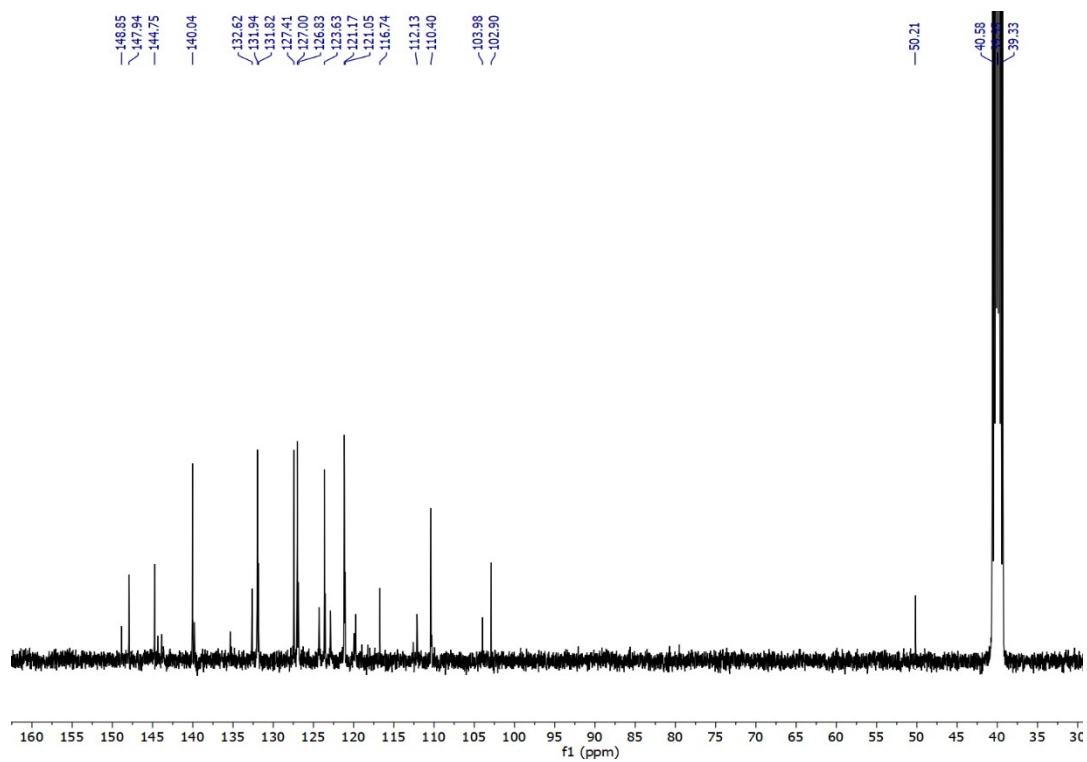


Figure S2: ^{13}C NMR (75 MHz) spectra of the receptor (CPI) in DMSO-d_6 .

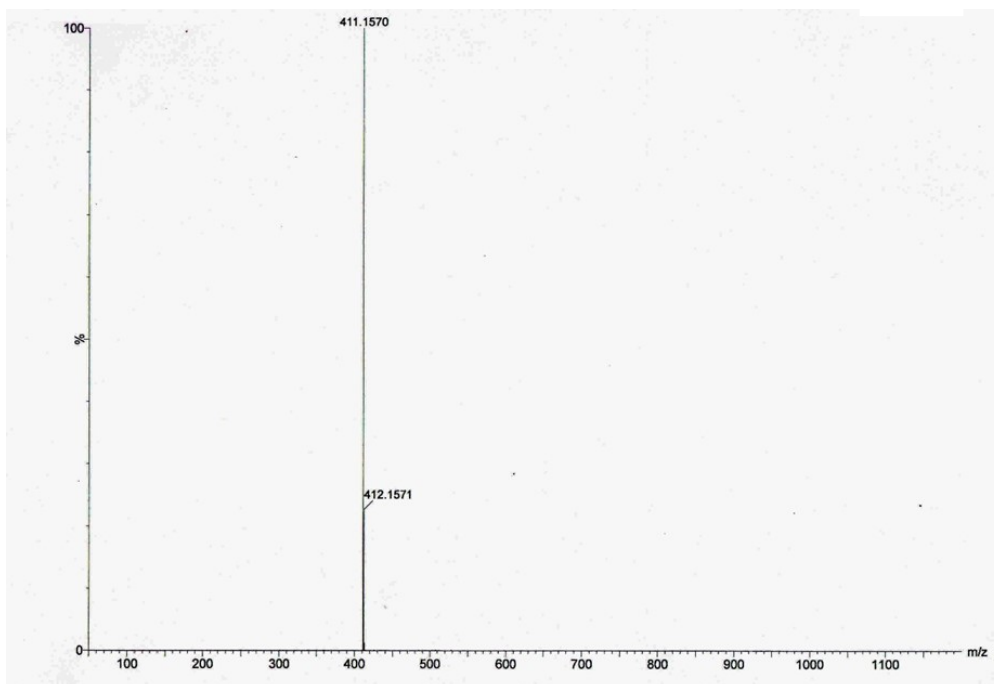


Figure S3: HRMS of the receptor (CPI)

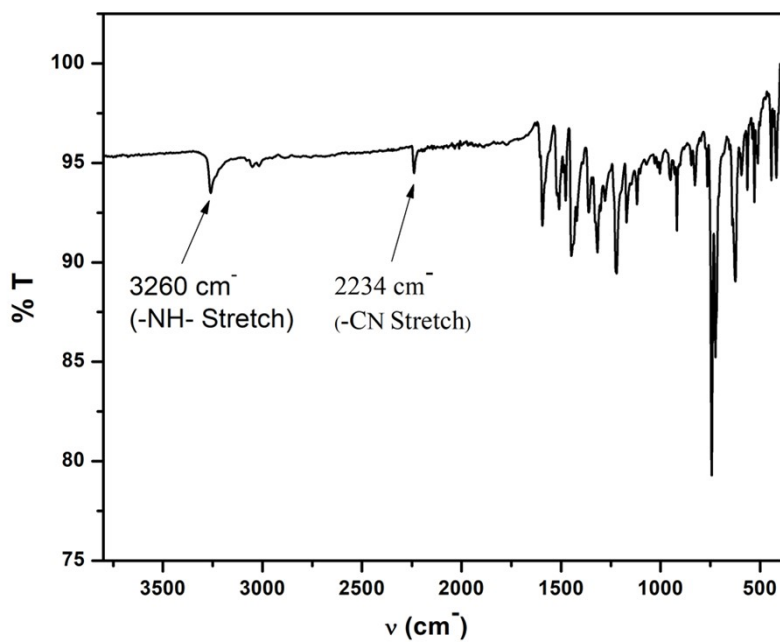


Figure S4: FTIR Spectrum of CPI

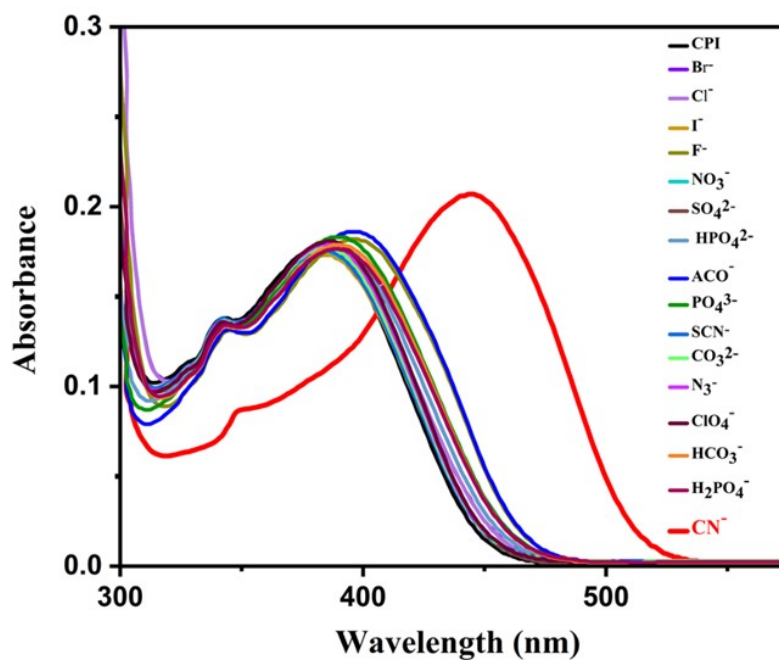


Figure S5: UV-Vis spectra of CPI (20 μM) upon addition of different anions (40 μM) such as F^- , Cl^- , Br^- , I^- , ACO^- , NO_3^- , CO_3^{2-} , SCN^- , HCO_3^- , N_3^- , HSO_4^- , SO_4^{2-} , H_2PO_4^- , HPO_4^{2-} and PO_4^{3-} in DMSO.

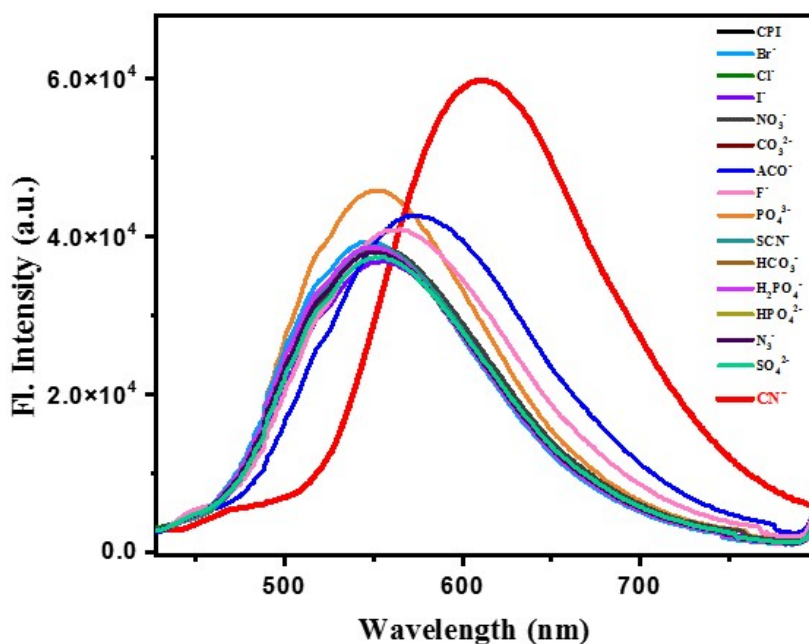


Figure S6: Emission spectra of CPI (20 μM) upon addition of various anions (40 μM) such as F^- , Cl^- , Br^- , I^- , ACO^- , NO_3^- , CO_3^{2-} , SCN^- , HCO_3^- , N_3^- , HSO_4^- , SO_4^{2-} , H_2PO_4^- , HPO_4^{2-} and PO_4^{3-} in DMSO.

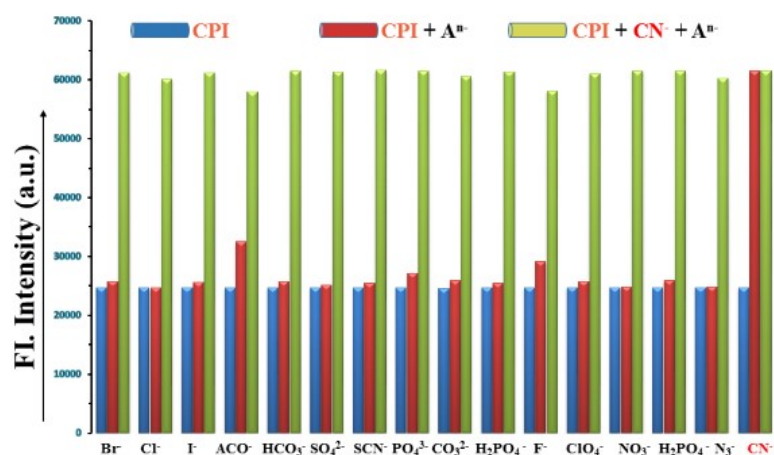


Figure S7: Competitive experiments of CPI (20 μM) for CN^- (40 μM) in presence of common anions (40 μM). Fluorescence intensity at 625 nm for CPI itself (20 μM) (blue bar), with various coexisting anions (40 μM , red bar) such as F^- , Cl^- , Br^- , I^- , ACO^- , NO_3^- , CO_3^{2-} , SCN^- , HCO_3^- , N_3^- , HSO_4^- , SO_4^{2-} , H_2PO_4^- , HPO_4^{2-} and PO_4^{3-} and upon subsequent addition of CN^- (40 μM) (green bar); $\lambda_{\text{ex}} = 410 \text{ nm}$.

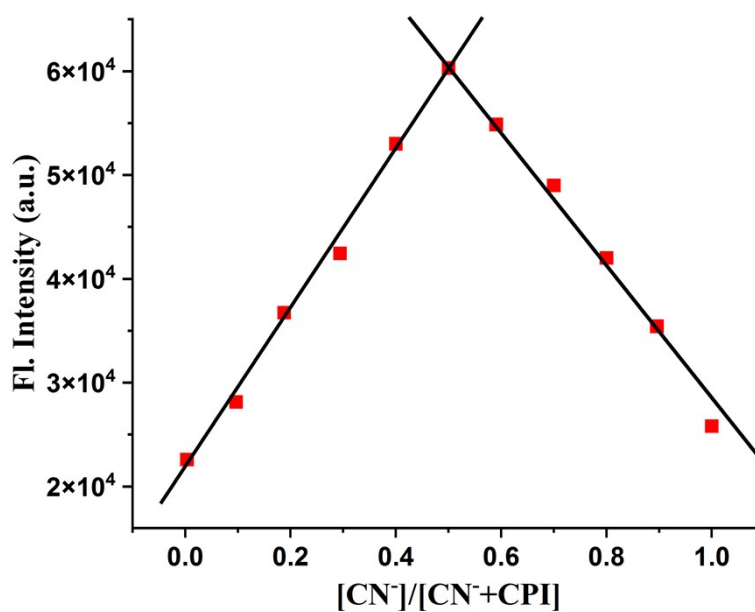


Figure S8: Stoichiometry plot for CPI- CN^- adduct formation by recording fluorescence intensity changes at 625 nm ($\lambda_{\text{ex}} = 410 \text{ nm}$).

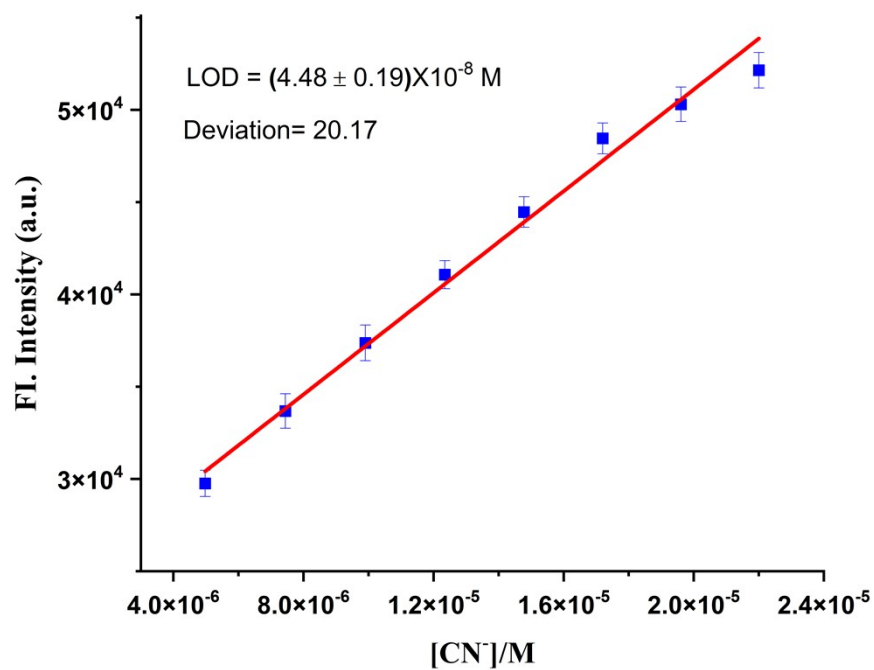
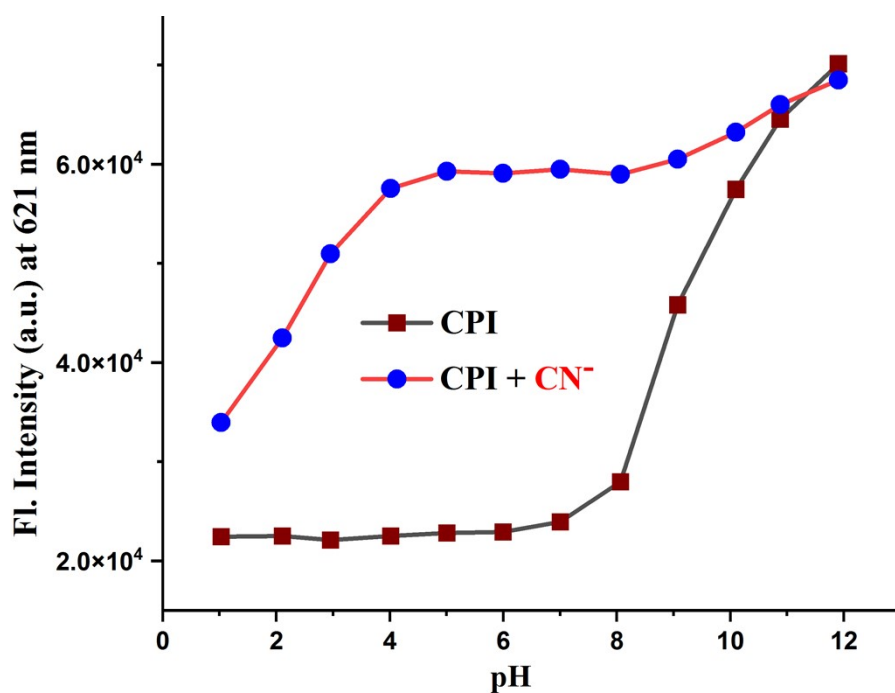


Figure S9: Linear response curve of CPI at 625 nm depending on the CN⁻ concentration.



- **Figure S10:** Fluorescence response of CPI and CPI-CN⁻ as a function of pH. Fluorescence intensities were recorded within the pH range of 0 to 12.

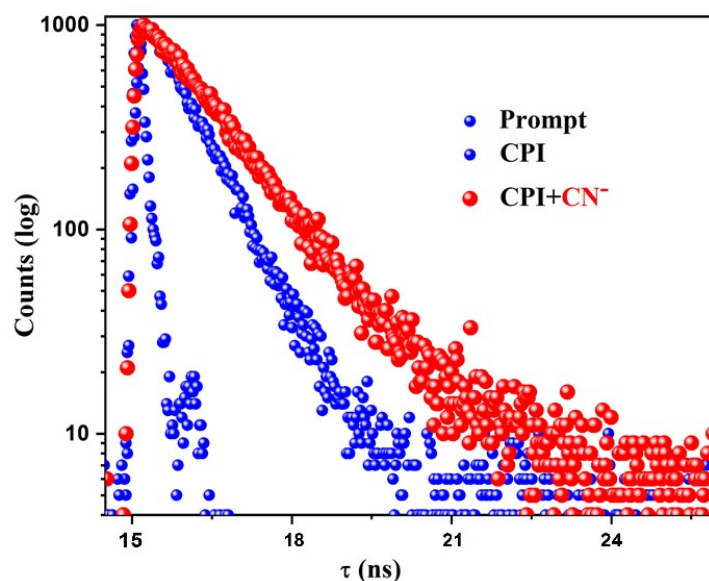


Figure S11: Lifetime decay profile of CPI (●●●) and CPI-CN⁻ adduct (●●●).

Determination of fluorescence Quantum Yields (Φ) of CPI and its adduct with CN⁻

The luminescence quantum yield was determined using coumarin-153 as reference dye. The compounds and the reference dye were excited at the similar wavelength and the emission spectra were then studied. The area of the emission spectrum was integrated and the quantum yield is determined according to the following equation:

$$\phi_S/\phi_R = [A_S / A_R] \times [(Abs)_R / (Abs)_S] \times [n_S^2/n_R^2]$$

Here, ϕ_S and ϕ_R are the luminescence quantum yields of the sample and reference dye, respectively. A_S and A_R are the area under the emission spectra of the sample and the reference respectively, $(Abs)_S$ and $(Abs)_R$ are the respective optical densities of the sample and the reference solution at the wavelength of excitation, and n_S and n_R stand for the values of refractive index for the respective solvent used for the sample and reference.

The quantum yields of CPI and CPI-CN⁻ are determined using the above mentioned equation and the values are found to be 0.225 and 0.305 respectively. Radiative rate constant K_r and total non radiative rate constant K_{nr} have been calculated using the equation $\tau^{-1} = K_r + K_{nr}$ and $K_r = \phi_f / \tau$ (Table. S1).

Table S1: Determination of Fluorescence life-time data, quantum yield, radiative and non-radiative rate constants

Compd.	Quantum yield(ϕ)	τ (ns)	$K_r(10^8 \times S^{-1})$	$K_{nr}(10^8 \times S^{-1})$
CPI	0.225	2.95	0.7627	2.6271
CPI-CN⁻	0.305	3.51	0.8689	1.9801

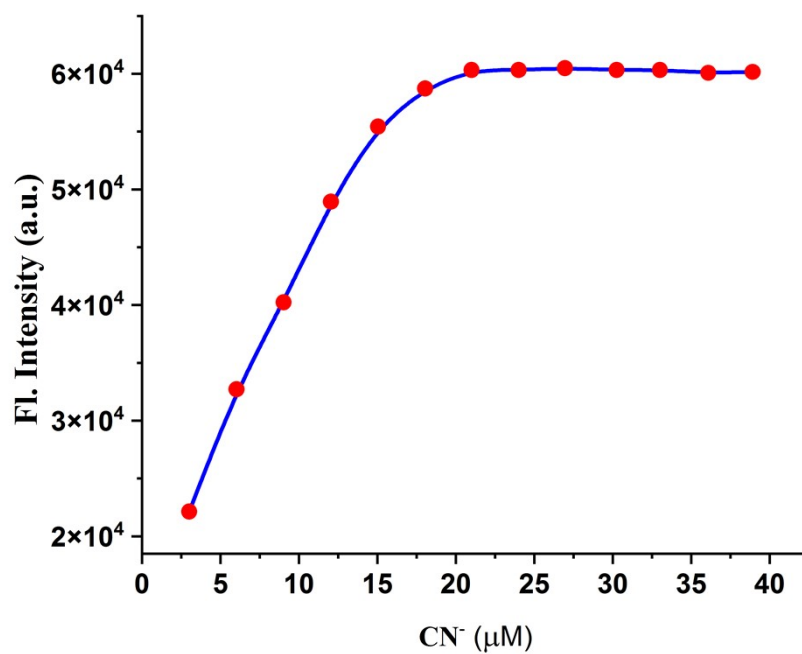


Figure S12. Mole ratio plot of CPI (20 μM) for CN⁻ (40 μM) at 625 nm using fluorescence titration method (λ_{ex} = 410 nm).

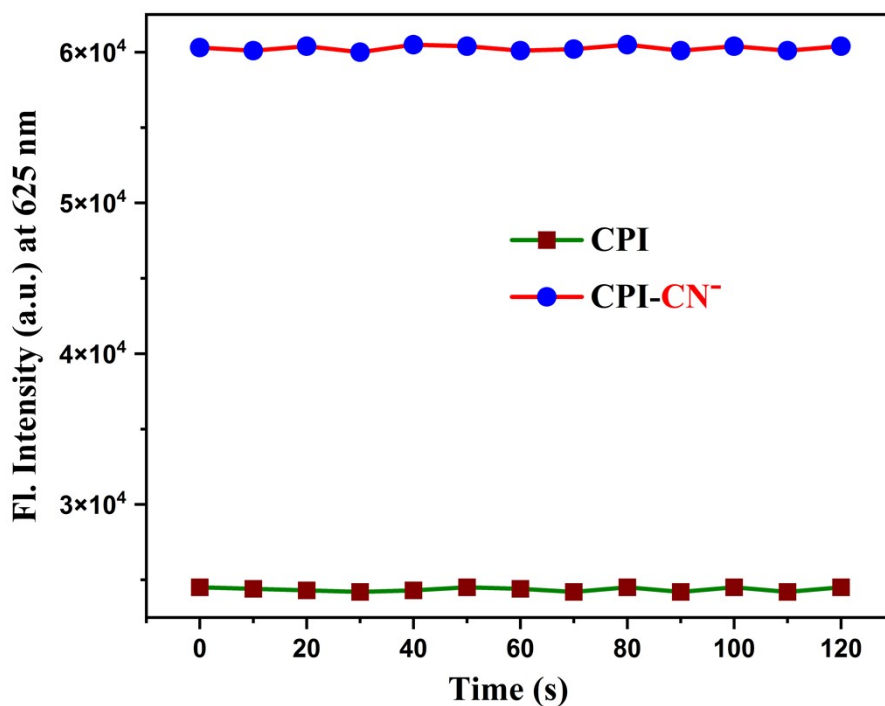


Figure S13. Photostability plot of CPI and CPI-CN⁻ adduct obtained within 0-2 min time interval in DMSO solution. The change in fluorescence intensity was recorded at 625 nm upon excitation at 410 nm.

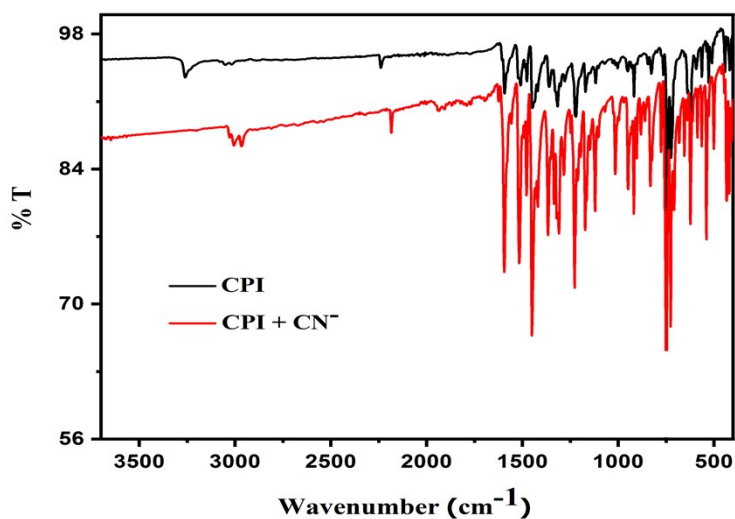


Figure S14. FTIR spectra of CPI (black line) and CPI-CN⁻ (red line)

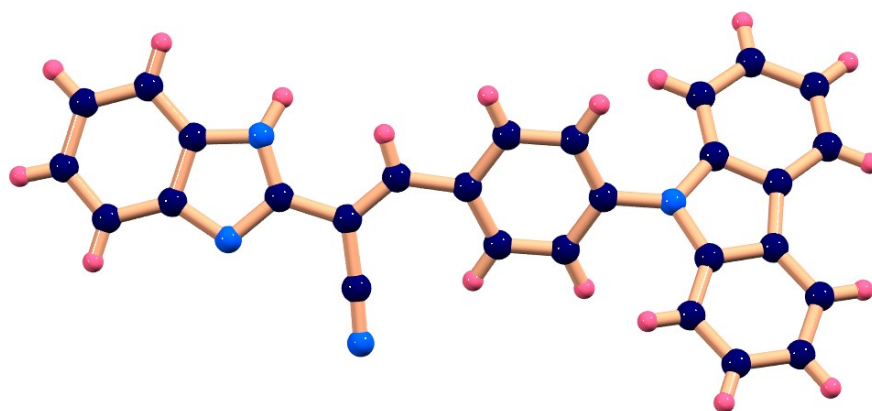


Figure S15. Optimized structure of CPI calculated by DFT/B3LYP/6-31+G(d) method.

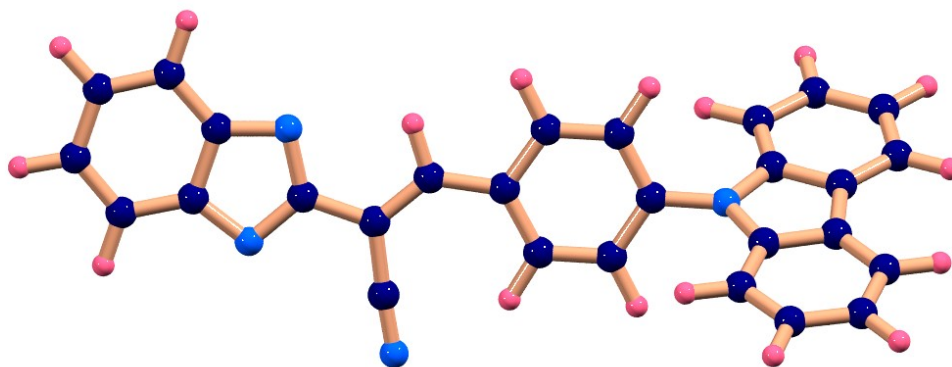


Figure S16. Optimized structure of CPI⁻ calculated by DFT/B3LYP/6-31+G(d) method.

Table S2. Crystallographic data and refinement parameters of the sensor (**CPI**)

Chemical formula	C ₂₈ H ₁₈ N ₄
Formula weight	410.46
Temperature of study	293(2)
Crystal system	<i>orthorhombic</i>
Space group	<i>Pbca</i>
a, b, c [Å]	9.1730(7), 19.8496(16), 25.741(2)
α / β / γ [°]	90
V [Å ³]	4686.9(7)
Z	8
D(calc) [g/cm ³]	1.163
Mu(MoKa) [/mm]	0.070
Radiation [Å]	0.71073
F(000)	1712
θ (Min-Max) [°]	2.052-25.048
Dataset (h; k; l)	-10 to 10, -21 to 23, -25 to 30
Total collected data	32712
Unique data [R _{int}]	4130 [0.0674]
Refined parameters	325
R, wR ₂	0.0813, 0.2197
Goodness of fit	1.034
Residual density	-0.346/0.403
CCDC Number	2287312

Table S3. Selected X-ray and calculated bond distances and angles of the sensor (**CPI**)

Bonds(Å)	X-ray	Calc.
N1 – C1	1.364(4)	1.31654
N1 – C7	1.383(4)	1.38191
N2 – C1	1.312(4)	1.38581
N2 – C2	1.386(4)	1.38391
N3 – C9	1.140(5)	1.16337
C1 – C8	1.463(4)	1.46462
C8 – C9	1.434(5)	1.43369
C8 – C10	1.339(5)	1.36552
C10 – C11	1.452(4)	1.45505
Angles(°)	X-ray	Calc.
C1–N1–C7	106.5(3)	105.36614
C1–N2–C2	105.5(3)	106.99332
N2–C1–N1	112.8(3)	112.61983
N2–C1–C8	124.8(3)	123.45340
N1–C1–C8	122.4(3)	123.92247
C10–C8–C9	122.7(3)	123.09967
C10–C8–C1	122.2(3)	122.51273
C9–C8–C1	115.2(3)	114.38222
N3–C9–C8	176.9(4)	178.70198

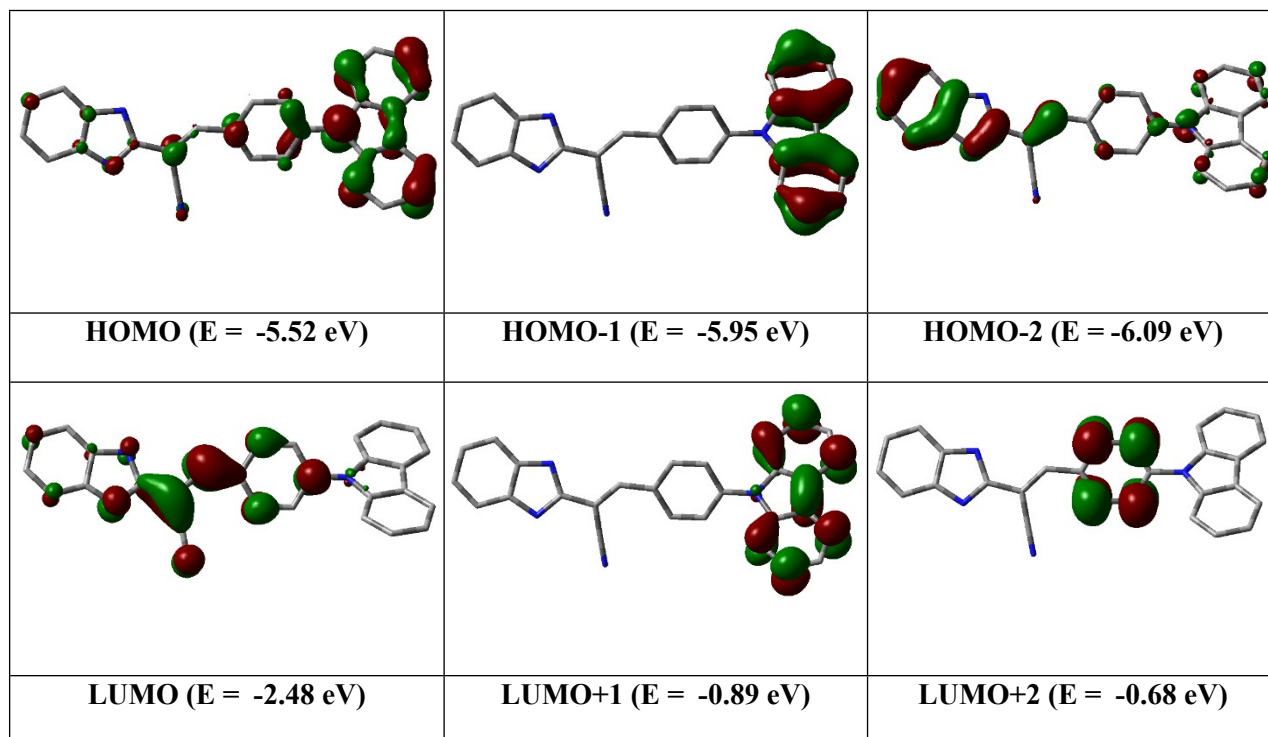


Figure S17. Contour plots of some selected molecular orbitals of CPI

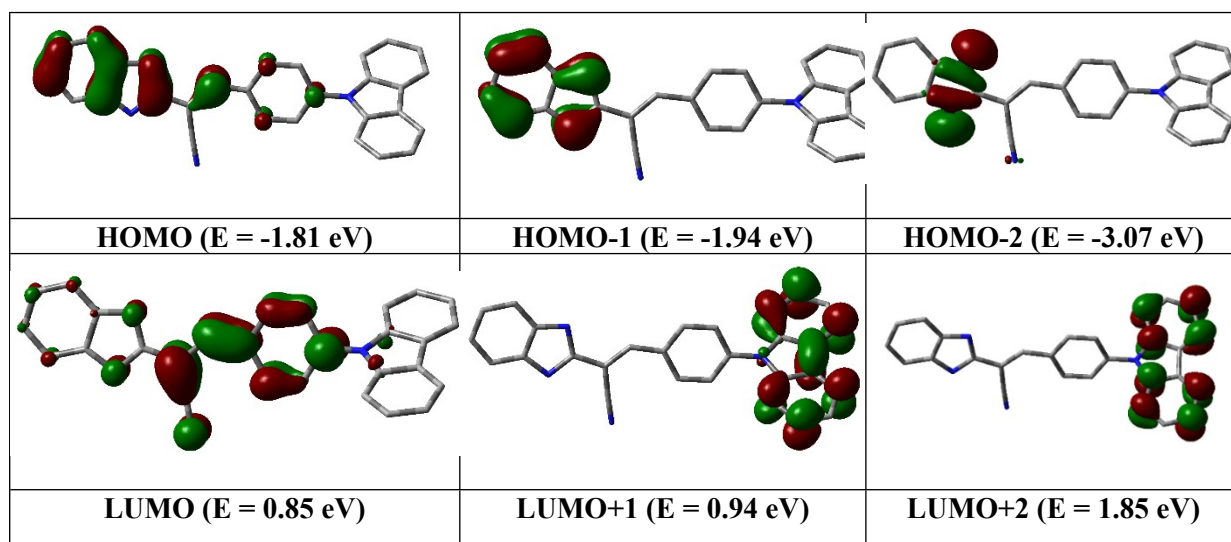
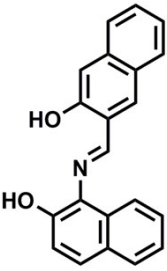
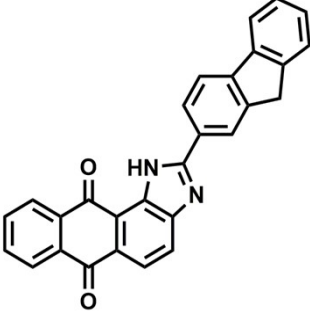
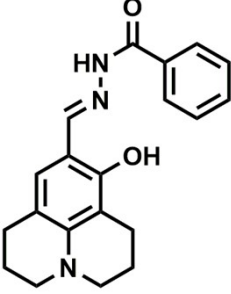


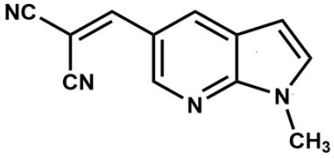
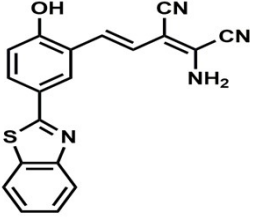
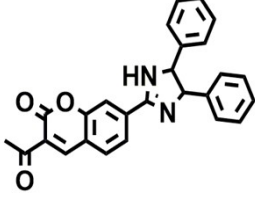
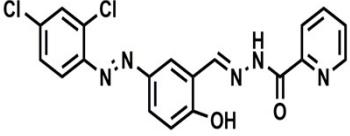
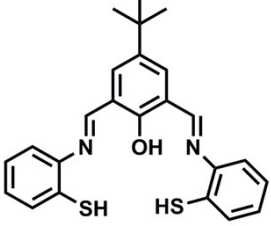
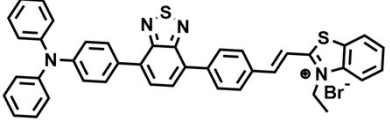
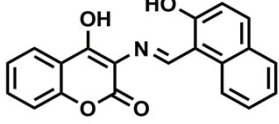
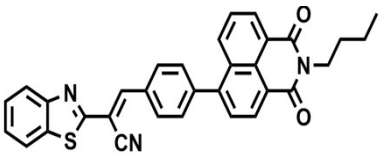
Figure S18. Contour plots of some selected molecular orbitals of CPI

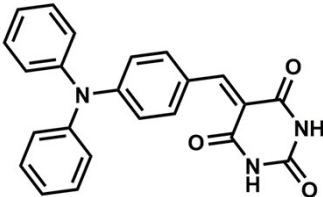
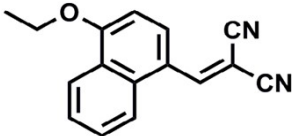
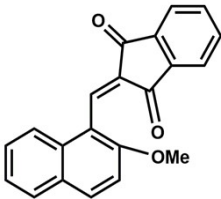
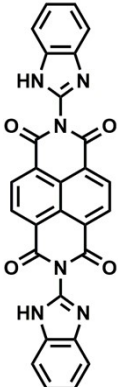
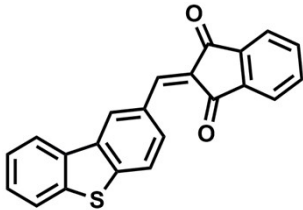
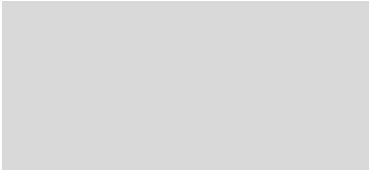
Table S4. Vertical electronic transitions of CPI and CPI⁻ calculated by TDDFT/CPCM method

Compd.	λ (nm)	E (eV)	Osc. Strength (f)	Key excitations	Character
CPI	468.32	2.6474	0.7727	(99%) HOMO→LUMO	$\pi \rightarrow \pi^*$
	377.16	3.2873	0.5368	(97%) HOMO-2→LUMO	$\pi \rightarrow \pi^*$
CPI⁻	473.41	2.6189	0.7941	(85%) HOMO→LUMO	$\pi \rightarrow \pi^*$
	448.02	2.7674	0.3516	(86%) HOMO-1→LUMO	$\pi \rightarrow \pi^*$

Table S5: Sensing performance of CPI towards CN⁻ compared to other previously reported receptors.

Probe	Solvent System	Detection limit	Reaction time	Reference
	DMF:H ₂ O (1:1, v/v)	0.21 μ M		[1]
	CH ₃ CN-H ₂ O(8:2, pH=3-10)	4.11x10 ⁻⁸ M		[2]
	CH ₃ CN-H ₂ O (v/v, 19:1)	9.4x10 ⁻¹⁰ M		[3]

	THF-H ₂ O (9:1)	2×10 ⁻⁶ M		[4]
	DMSO/H ₂ O(7:3)	1.4x10 ⁻⁷ M		[5]
	Dioxane	1.0 μM	Within 60 s	[6]
	DMSO-H ₂ O (6:4,v/v), pH=7.1	6.4 μM		[7]
	DMSO-H ₂ O (20-80% v/v)	0.96 μM		[8]
	H ₂ O/THF(8:2)	1.3x10 ⁻⁷ M		[9]
	DMSO	0.11 μM		[10]
	THF	0.034 μM		[11]

	DMSO/H ₂ O (1:99)	2.95x10 ⁻⁸ M		[12]
	THF-H ₂ O (9:1, V/V), HEPES Buffer, pH=7.3	1.1x10 ⁻⁶ M		[13]
	H ₂ O-DMF(9:1,v/v)	1.15-1.2 nM	10-30 sec	[14]
	DMSO-H ₂ O (9:1, V/V), HEPES Buffer, pH=6-9	8.32x10 ⁻⁷ M	Less than 1 min	[15]
	DMSO/H ₂ O (1:99,v/v)	2.26x10 ⁻⁷ M	15 sec	[16]
	DMSO	4.48x10 ⁻⁸ M	50 sec	Present work

References

1. B. Yilmaz, M. Keskinates, Z. Aydin and M. Bayrakci, A highly selective optical sensor for the detection of cyanide ions in aqueous solution and living cells, *J. Photochem. Photobiol. A*, 2022, **424**, 113651.
2. R. Bhaskar, V. Vijayakumar, V. Srinivasadesikan, S. Lee and S. Sarveswari, Rationally designed imidazole derivative as colorimetric and fluorometric sensor for selective, qualitative and quantitative cyanide ion detection in real time samples, *Spectrochim. Acta A*, 2020, **234**, 118212.
3. C.-B. Bai, J. Zhang, R. Qiao, Q.-Y. Zhang, M.-Y. Mei, M.-Y. Chen, B. Wei, C.-Q. Wang and C. Qu, Reversible and selective turn on fluorescent and naked-eye colorimetric sensor to detect cyanide in tap water, food samples, and living systems, *Ind. Eng. Chem. Res.*, 2020, **59**, 8125-8135.
4. K.-Y. Chen and W.-C. Lin, A simple 7-azaindole-based ratiometric fluorescent sensor for detection of cyanide in aqueous media, *Dyes Pigm.*, 2015, **123**, 1-7.
5. S. Malkondu, S. Erdemir and S. Karakurt, Red and blue emitting fluorescent probe for cyanide and hypochlorite ions: Biological sensing and environmental analysis, *Dyes Pigm.*, 2020, **174**, 108019.
6. R. Ali, S. K. Dwivedi, H. Mishra and A. Misra, Imidazole-Coumarin containing D-A type fluorescent probe: synthesis photophysical properties and sensing behaviour for F⁻ and CN⁻ anions, *Dyes Pigm.*, 2020, **175**, 108163.
7. Z. Li, C. Liu, S. Wang, L. Xiao and X. Jing, Visual detection of cyanide ion in aqueous medium by a new chromogenic azo-azomethine chemosensor, *Spectrochim. Acta A*, 2018, **210**, 321-328.
8. P. S. Kumar, P. R. Lakshmi and K. P. Elango, An easy to make chemoreceptor for the selective ratiometric fluorescent detection of cyanide in aqueous solution and in food materials, *New J. Chem.*, 2019, **43**, 675.
9. B. Zhai, Z. Hu, C. Peng, B. Liu, W. Li and C. Gao, Rational design of a colorimetric and fluorescence turn-on chemosensor with benzothiazolium moiety for cyanide detection in aqueous solution, *Spectrochim. Acta A*, 2020, **224**, 117409.
10. Z. Aydin, M. Keskinates, B. Yilmaz, M. Durmaz and M. Bayrakci, A rapid responsive coumarin-naphthalene derivative for the detection of cyanide ions in cell culture, *Anal. Biochem.*, 2022, **654**, 114798.
11. T. S. Reddy, H. Moon and M. S. Choi, Turn-on fluorescent naphthalimide-benzothiazole probe for cyanide detection and its two-mode aggregation-induced emission behavior, *Spectrochim. Acta A*, 2021, **252**, 119535.
12. B. Zuo, L. Liu, X. Feng, D. Li, W. Li, M. Li, M. Huang and Q. Deng, A novel fluorescent sensor based on triphenylamine with AIE properties for the highly sensitive detection of CN⁻, *Dyes Pigm.*, 2021, **193**, 109534.
13. S. D. Padghan, C. Wang, W. Liu, S. Sun, K. Liu and K. Chen, A naphthalene-based colorimetric and fluorometric dual-channel chemodosimeter for sensing cyanide in a wide pH rang, *Dyes Pigm.*, 2020, **183**, 108724.
14. N. Maurya and A. K. Singh, Selective naked eye and "turn-on" fluorescence chemodosimeter for CN⁻ by activated Michael acceptor possessing different polar substituents: reduced ICT-based signal transduction, *Sens. Actuators, B*, 2017, **245**, 74-80.
15. Q. Lin, L. Liu, F. Zheng, P. Mao, J. Liu, Y. Zhang, H. Yao and T. Wei, A benzimidazole functionalized NDI derivative for recyclable fluorescent detection of cyanide in water, *RSC Adv.*, 2017, **7**, 38458.
16. Q. Zou, J. Du, C. Gu, D. Zhang, F. Tao and Y. Cui, A new dibenzothiophene-based dual channel chemosensor for cyanide with aggregation induced emission, *J. Photochem. Photobiol. A*, 2021, **405**, 112993.